Journal of Materials Chemistry B

PAPER

View Article Online
View Journal | View Issue

Cite this: *J. Mater. Chem. B*, 2019, 7, 6789

Antimony selenide/graphene oxide composite for sensitive photoelectrochemical detection of DNA methyltransferase activity†

Huaijia Xue, Kaiyang Chen, Qing Zhou, Deng Pan, Yuanjian Zhang and Yanfei Shen *

Received 24th July 2019,
Accepted 25th September 2019

DOI: 10.1039/c9tb01541h

rsc.li/materials-b

Antimony selenide (Sb_2Se_3) as a p-type semiconductor material has recently attracted extensive attention for its excellent photoelectric properties in applications of thin film solar cells. However, applying Sb_2Se_3 as a photoelectrochemically (PEC) active material for constructing biosensors has never been reported. In this work, by using Sb_2Se_3/graphene oxide (Sb_2Se_3–GO) as both the PEC probe and substrate for biomolecule conjugation, a "signal-off" sandwich-type PEC biosensor was proposed for DNA methyltransferase (Dam MTase) activity detection based on gold nanoparticles (Au NPs) as quenchers. In the presence of Dam MTase and Dpn I, hairpin probe DNA (hDNA) was cleaved into single-stranded DNA (ssDNA), which could be hybridized with Au NP-functionalized DNA (S1) to form a double-stranded DNA (dsDNA) complex. The formation of dsDNA shortened the distance between Au NPs and Sb_2Se_3 on the electrode and induced competitive absorption and exciton energy transfer (EET) between Sb_2Se_3 and the Au NPs, thus significantly reducing the photocurrent. The constructed PEC biosensor exhibited a superior performance compared to most reports with a wide detection range from 1 mU mL^{-1} to 100 U mL^{-1} and a low detection limit of 0.6 mU mL^{-1} for the detection of Dam MTase. This work opens a new avenue for Sb_2Se_3 in biosensing applications and provides a new technology for the early warning and early diagnosis of diseases.

Introduction

Tumor formation is mainly influenced by genetic modification and epigenetic modification. DNA methylation is an epigenetic modification that regulates the growth and development of individuals under the catalysis of DNA methyltransferase (Dam MTase).[1,2] Related studies have shown that abnormal DNA methylation, *i.e.*, an imbalance in Dam MTase activity, is associated with cancer.[3] An in-depth study of Dam MTase activity can provide valuable guidance for clinical diagnosis and cancer therapy. Traditional methods for DNA MTase determination include radiolabeling of DNA substrates,[4] high-performance liquid chromatography,[5] and gel electrophoresis.[6] However, these assays require long assay procedures, expensive instruments, and unsafe isotope labeling, which limits their practical application. Therefore, it is still challenging to develop a highly sensitive, simple and rapid method for the detection of Dam MTase activity. Compared to these traditional methods, photoelectrochemical (PEC) sensors have attracted more attention due to the complete separation of excitation light and detection signal, which not only reduces the background current to improve sensitivity but also enhances selectivity.[7–10]

Antimony selenide (Sb_2Se_3), a p-type semiconductor material with a narrow band gap (1.0–1.3 eV), has recently drawn extensive attention for its excellent photoelectric and thermoelectric properties.[11,12] Moreover, Sb_2Se_3 is stable and composed of inexpensive and earth-abundant components, Sb and Se.[13] These unique properties of Sb_2Se_3 make it promising for applications requiring highly efficient, low-toxicity, stable and inexpensive photoelectric materials in both energy and biosensing fields. After Tang's group successfully applied Sb_2Se_3 in thin-film solar cells, an Sb_2Se_3 photocathode was also developed for PEC water splitting.[14–16] Jooho Moon's group demonstrated that a photocathode composed of Sb_2Se_3 nanoneedles modified with TiO_2 and Pt can be used to produce hydrogen from a PEC.[17] Overall, the excellent photoelectric, low-toxic and inexpensive properties of Sb_2Se_3 are worth extensive research for further applications. However, applying Sb_2Se_3 as a PEC probe for constructing biosensors has never been reported.

Herein, we report the utilization of Sb_2Se_3 as a highly efficient PEC probe and Au NPs as a quencher to construct a sandwich-type PEC biosensor based on the wide absorption in

Medical School, School of Chemistry and Chemical Engineering, Southeast University, Nanjing 210009, China. E-mail: Yanfei.Shen@seu.edu.cn

† Electronic supplementary information (ESI) available. See DOI: 10.1039/c9tb01541h

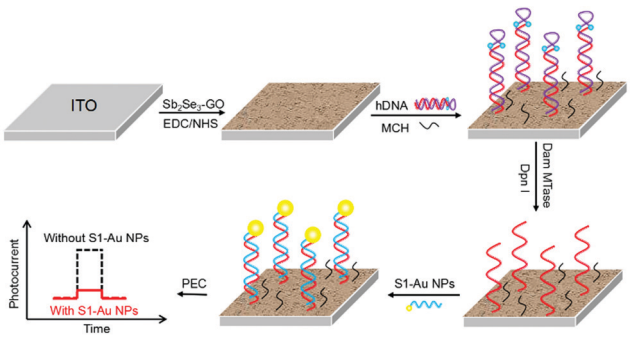

Fig. 1 Schematic diagram of the proposed PEC biosensor construction for Dam MTase activity detection.

the UV-vis region and the high PEC efficiency of Sb_2Se_3. Due to the competitive absorption of light and exciton energy transfer (EET) between Sb_2Se_3 and Au NPs, the Au NPs exhibited an obvious quenching effect towards Sb_2Se_3 on the photoelectrode (Fig. 1). To enhance the biological compatibility and provide more active sites for biomolecule conjugation, Sb_2Se_3 was further modified with graphene oxide (GO). By taking Dam MTase as a model cancer biomarker, the constructed PEC biosensor showed high stability and sensitivity. This work opens a new avenue for PEC biosensing by using Sb_2Se_3 as a new probe, which could provide a new platform for applications in the early diagnosis and treatment of diseases.

Results and discussion

Characterization of the Sb_2Se_3 and Sb_2Se_3–GO nanostructure

The morphology and structure of the prepared Sb_2Se_3 and Sb_2Se_3–graphene oxide (GO) were first characterized using scanning electron microscopy (SEM) images and energy dispersive spectroscopy (EDS) spectra. Fig. 2a shows that Sb_2Se_3 consists of spherical nanoparticles with a rough surface and an average particle size of approximately 650 nm. The EDS spectrum (Fig. 2b) of Sb_2Se_3 shows that the material consists of Sb and Se, and the atomic ratio of Sb and Se was close to 2 : 3, which indicates that Sb_2Se_3 was successfully prepared. X-ray photoelectron spectroscopy (XPS) analysis was further carried out to gain more information. An XPS spectrum of the Sb_2Se_3 sample at 0–1350 eV is shown in Fig. 3a. Except for the Si (180.7 eV) characteristic peak (tested using a prepared silicon wafer), only the characteristic peaks of Sb and Se were present, indicating that the prepared sample was pure and free of other impurities. No oxygen peak (532.91 eV) was observed in Fig. 3a, indicating that Sb_2Se_3 was not oxidized.[18] The binding energy values were 33.13 eV for Sb $4d_{5/2}$, 34.53 eV for Sb $4d_{3/2}$ (Fig. 3c), 55.88 eV for Se $3d_{5/2}$ and 55.73 eV for Se $3d_{3/2}$ in Sb_2Se_3 (Fig. 3d), which is consistent with previous reports,[19,20] indicating the successful synthesis of Sb_2Se_3.

To increase the water dispersibility of Sb_2Se_3 and provide sufficient conjugation sites for biomolecules, an Sb_2Se_3–GO nanohybrid was prepared.[21] As shown in Fig. 2a and c, when Sb_2Se_3 was assembled with GO, the surfaces of the spherical

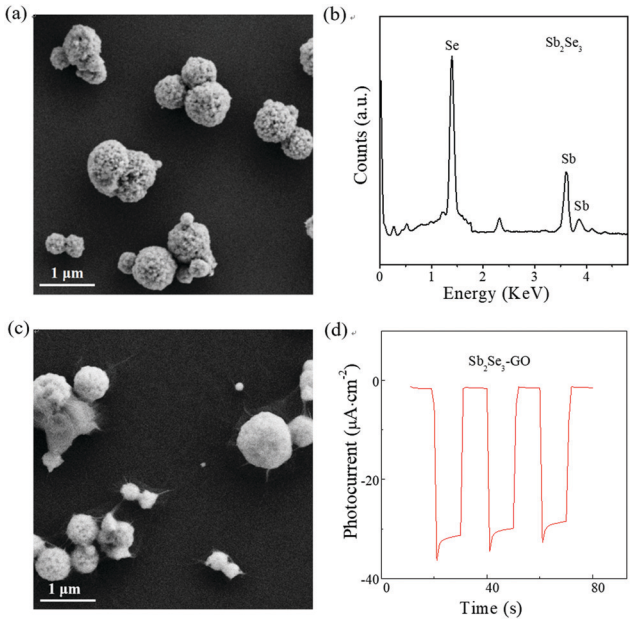

Fig. 2 SEM image (a) and EDS spectrum (b) of Sb_2Se_3, and SEM image (c) and photocurrent response (d) of Sb_2Se_3–GO.

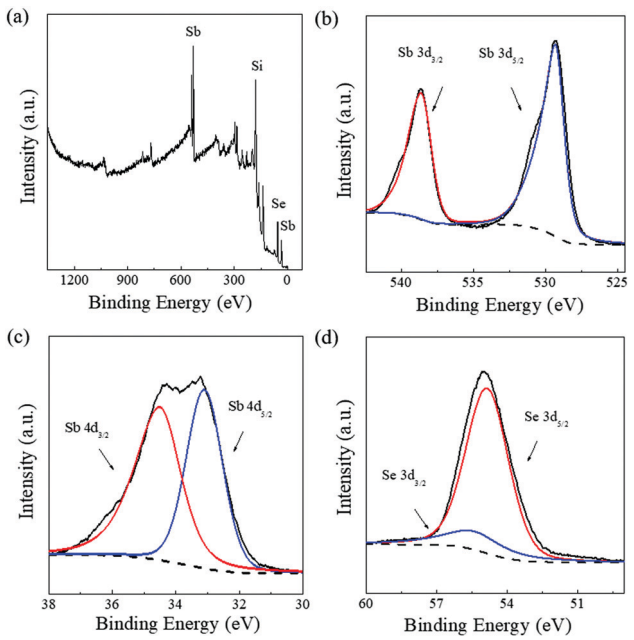

Fig. 3 XPS spectra of Sb_2Se_3: full spectrum (a), Sb 3d (b), Sb 4d (c) and Se 3d (d). The XPS samples were prepared with a silicon wafer as a substrate.

Sb_2Se_3 nanoparticles were uniformly covered with a transparent film, which is the topographical structure of GO, demonstrating the successful preparation of the Sb_2Se_3–GO nanohybrid. Moreover, as shown in Fig. S1 (ESI†), ultraviolet-visible (UV-vis) absorption spectra showed that the Sb_2Se_3–GO nanohybrid had wide absorption in the whole UV-vis region with a maximum absorption at 230 nm, which was correlated to the sum of the absorption values for GO and Sb_2Se_3, suggesting the successful preparation of the Sb_2Se_3–GO nanohybrid. The formation of the nanohybrid could be

ascribed to the interaction between Sb and oxygen-containing functional groups in GO and electron interaction between GO and Sb_2Se_3.[22] To evaluate the photoelectric activity of the Sb_2Se_3–GO nanohybrid, a standard PEC cell was constructed to measure the photocurrent generated under chopped light irradiation. As shown in Fig. 2d, the photocurrents were prompt, steady, and reproducible under the chopped light. Thus, the Sb_2Se_3–GO nanohybrid is a desirable PEC probe for the construction of highly sensitive biosensors.

Feasibility and mechanism of the constructed PEC biosensors

Based on its excellent photoelectric properties, Sb_2Se_3 was used as a PEC probe for the fabrication of PEC sensors. After the modification of the electrode with Sb_2Se_3–GO, hairpin DNA (hDNA) was covalently bound to the GO by amide bonds. Upon catalysis by Dam MTase at the recognition site (5′-GATC-3′), the hDNA was methylated, and restriction endonuclease (Dpn I) can effectively recognize the 5′-GATC-3′ sequence and cleave adenine methylated hDNA to release single-stranded DNA (ssDNA). After that, gold nanoparticle (Au NP)-functionalized DNA (S1) could hybridize with the ssDNA on the electrodes, resulting in a double-stranded DNA (dsDNA) complex that closed the distance between the Au NPs and Sb_2Se_3 on the electrode and induced competitive absorption and EET between the Sb_2Se_3 and the Au NPs, thus significantly reducing the photocurrent. To verify the feasibility of the constructed PEC sensor, a control experiment was performed by incubating the Dpn I/Dam/hDNA/Sb_2Se_3–GO/ITO electrode with merely S1 instead of the S1-Au NPs used for the fabrication of the PEC sensor. It can be clearly seen from Fig. 4a that the photocurrent reduction ratio $\Delta I/I_0$ of the S1-modified electrode was significantly lower than that of the S1-Au NP-modified electrode, indicating that Au NPs can act as a quencher of Sb_2Se_3 for the construction of a "signal-off" sensor.

To investigate the quenching mechanism of the signal-off PEC sensor, *i.e.*, the quenching effect of Au NPs on Sb_2Se_3 on the electrode substrate, UV-vis and fluorescence spectra were studied. The UV-vis spectra of Sb_2Se_3 and Au NPs, as shown in Fig. 4b, revealed that Sb_2Se_3 had a broad absorption in the wavelength range from 300 nm to 650 nm, while Au NPs also exhibited a broad absorption in the same range with an absorption peak centered at 512 nm.[23] In addition, when the concentration of Au NPs (39 μg mL^{-1}) was slightly lower than that of Sb_2Se_3 (48 μg mL^{-1}), the absorption of the Au NPs was much stronger than that of Sb_2Se_3, indicative of competitive absorption between Sb_2Se_3 and Au NPs under light irradiation. That is, when Au NPs were captured on the electrode, the absorption of Sb_2Se_3 was greatly reduced, which in turn led to a decrease in photocurrent generation. Furthermore, as shown in Fig. 4c, Sb_2Se_3 had a strong emission in the range of 390–445 nm with an emission peak centered at 399 nm. The spectral overlap between the fluorescent spectrum of Sb_2Se_3 and the absorption spectrum of Au NPs demonstrated the EET between Sb_2Se_3 and Au NPs.[24] As shown in Fig. 4d, the fluorescent intensity of Sb_2Se_3 showed a gradual reduction with the increase of the Au NP concentration in the Sb_2Se_3 solution, Therefore, the quenching mechanism of the "signal-off" PEC sensor can be ascribed to the following two factors: (1) competitive absorption between Sb_2Se_3 and Au NPs and (2) EET between Sb_2Se_3 and AuNPs. Both of the above quenching mechanisms effectively demonstrate that Au NPs can quench the PEC signal of Sb_2Se_3.

Fabrication of the PEC biosensor

The successful assembly of a PEC sensor directly affects the stability and sensitivity of the sensor. Thus, CV and PEC measurements were used to monitor each step in the construction process (Fig. 1). First, the PEC sensor was monitored by CV measurements in 10 mM PBS (pH 7.4) containing 2.0 mM $K_3[Fe(CN)_6]$ under the optimized experimental conditions (the optimization of experimental conditions is given in Fig. S2, ESI†). As shown in Fig. 5a, when the electrode was modified with

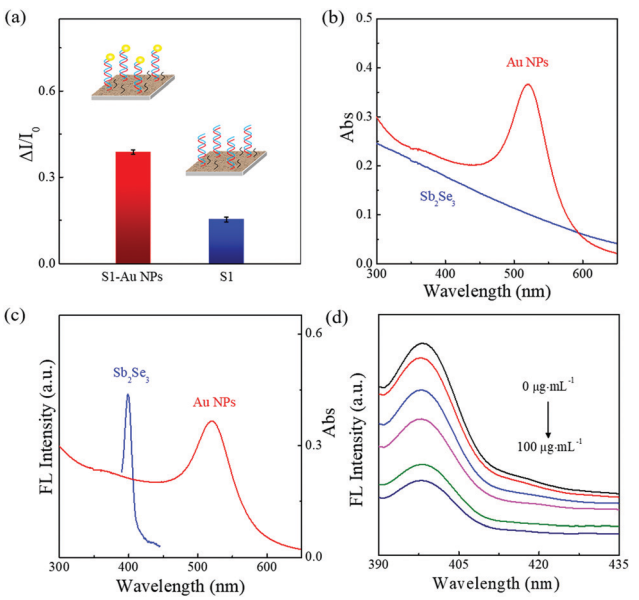

Fig. 4 (a) Photocurrent responses of S1-Au NP and S1-modified electrodes. (b) UV-vis absorption spectra of Sb_2Se_3 (48 μg mL^{-1}) and Au NPs (39 μg mL^{-1}). (c) Fluorescence spectrum of Sb_2Se_3 and UV-vis absorption spectrum of Au NPs. (d) Fluorescence spectra of Sb_2Se_3 (27 μg mL^{-1}) in the presence of different concentrations (0, 2, 20, 40, 80 and 100 μg mL^{-1}) of Au NPs.

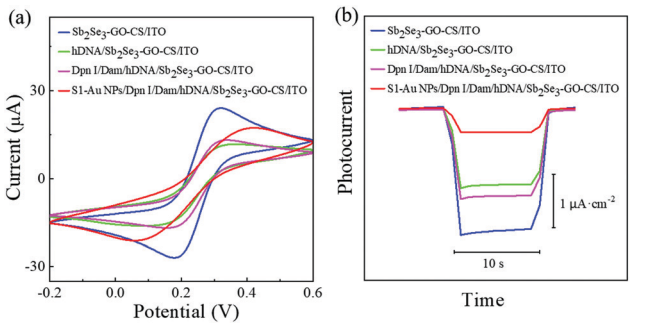

Fig. 5 (a) CV responses of the PEC biosensor-modified ITO after each step of assembly in 2.0 mM $K_3[Fe(CN)_6]$ solution. (b) Photocurrent responses of the PEC biosensor-modified ITO after each step of assembly in 10 mM PBS (pH = 6.0) solution with 0.1 M AA. The concentration of Dam MTase was 100 U mL^{-1}.

Sb_2Se_3–GO, a pair of well-defined redox peaks (blue curve) could be observed. When hDNA was further modified on the electrode, a significant decrease in the redox peak current (green curve) was observed due to the large steric hindrance of hDNA, which hindered electron transfer on the electrode surface. Subsequently, further treatment of the modified electrode with Dam MTase and Dpn I resulted in a slight enhancement in the peak current (magenta curve), which could be attributed to the cleavage of hDNA into ssDNA, inducing a decrease in steric hindrance on the electrode surface. Finally, when the electrode was further incubated with S1-Au NPs (red curve), the redox peak current increased again because the Au NPs accelerated the electron transfer between $[Fe(CN)_6]^{3-/4-}$ and the ITO electrode. Therefore, the successful construction of the PEC biosensor was verified by the change in peak current at each step by CV monitoring.

The successful fabrication of the sensor was further verified *via* PEC measurement. As shown in Fig. 5b, the Sb_2Se_3–GO/ITO electrode showed an obvious photocurrent response (blue curve), suggesting that Sb_2Se_3–GO is an excellent photoelectrically active material for constructing PEC sensors. The photocurrent was significantly reduced after hDNA modification of the electrode (green curve) due to the increased steric hindrance from hDNA, which blocked electron transfer between AA and the electrode. After treating the electrode with Dam MTase and Dpn I, the photocurrent slightly increased (magenta curve), suggesting that Dpn I successfully sheared the hDNA into ssDNA, which reduced the steric hindrance on the electrode surface. Further assembly of the electrode with S1-Au NPs led to a significant reduction in photocurrent (red curve). The photocurrent change could be ascribed to the introduction of Au NPs onto the electrode surface upon DNA hybridization, which probably induced the competitive absorption of light and EET between the Au NPs and Sb_2Se_3. In addition, the increased steric hindrance of the complex formed by hybridization might deplete photocurrent generation. This result was consistent with previous UV-vis and fluorescent results. Therefore, both the CV and PEC results demonstrated the successful construction of the PEC biosensor.

Assay of Dam MTase activity

It was speculated that after the sandwich hybridization reaction, the S1-Au NPs would be quantitatively captured upon DNA hybridization and the decrease in the PEC signal of Sb_2Se_3 would be related to the amount of captured S1-Au NPs, based on the quenching of Sb_2Se_3 by Au NPs. Since the amount of captured S1-Au NPs is correlated with the amount of Dam MTase, which induces the cleavage of hDNA into ssDNA, the decrease in photocurrent of Sb_2Se_3 on the modified electrode would depend on the amount of Dam MTase. As shown in Fig. 6a, with increased Dam MTase concentration, the quenching of the S1-Au NPs/Dpn I/Dam/hDNA/Sb_2Se_3–GO/ITO-modified electrode increased, and the corresponding photocurrent gradually decreased under the optimal experimental conditions. Fig. 6b shows a calibration curve with a good relationship between the photocurrent decrease ratio $\Delta I/I_0$ and the logarithmic concentration of Dam MTase in the range of 0.001–100 U mL^{-1}. Using linear fitting (R^2 = 0.988), the linear regression equation

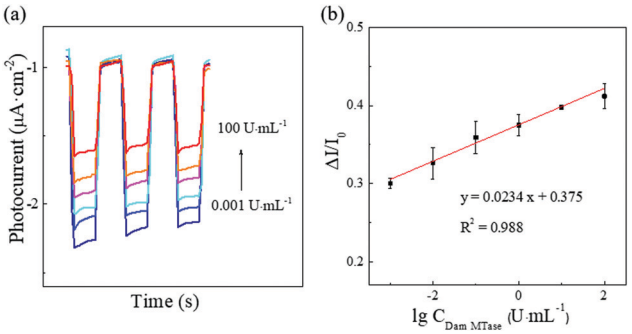

Fig. 6 (a) Photocurrent responses after incubation of Dpn I and (b) calibration curve of the PEC immunoassay for the detection of different concentrations of target Dam MTase from 1 mU mL^{-1} to 100 U mL^{-1}.

Table 1 Comparison of various methods for Dam MTase detection

Method	Linear range (U mL^{-1})	LOD (U mL^{-1})	Ref.
UV-vis	5–120	—	25
Differential pulse voltammetry	0.5–50	0.18	26
Differential pulse voltammetry	0.002–1	0.001	27
Fluorescence	0.1–40	0.06	28
Fluorescence	0.5–320	0.0085	29
Chemiluminescence	1–10	0.52	30
Electrochemistry	0.1–1	0.04	31
Electrochemiluminescence	0.1–100	0.03	32
Electrochemiluminescence	0.05–80	0.043	2
Electrochemiluminescence	0.001–100	0.00021	33
Linear sweep voltammetry	0.02–10	0.0073	34
PEC	0.04–64	0.015	35
PEC	0.001–100	0.0006	This work

was calculated as $\Delta I/I_0 = 0.0234 \lg C$ (U mL^{-1}) + 0.375, and the detection limit (LOD) was determined as 0.6 mU mL^{-1} according to the equation LOD = $3\sigma/S$, where σ represents the standard deviation of blank sample responses and S is the slope of the calibration curve. Moreover, the prepared PEC sensors showed superior performance compared to those in previous reports of Dam MTase detection (see Table 1), and further optimization of experimental conditions will be performed to improve the sensitivity and lower the error bar of the biosensor. Therefore, the high-performance ''signal-off'' PEC sensor using Sb_2Se_3 as a PEC probe and Au NPs as quenchers was very promising for the determination of Dam MTase activity.

Selectivity, reproducibility and stability of the Dam MTase assay

To evaluate the selectivity of the constructed PEC sensor for Dam MTase activity, M.SssI MTase was chosen as an interference protein, and only Dam MTase or Dpn I was selected as an interference control. M.SssI MTase can specifically recognize the sequence of 5′-CG-3′ embedded in dsDNA, which is different from the sequences recognized by Dam MTase (5′-GATC-3′). As shown in Fig. 7a, under the same experimental conditions, significant photocurrent reduction was observed in the presence of both Dam MTase and Dpn I, which was attributed to the highly specific recognition of Dam MTase and Dpn I towards hDNA. In contrast, the photocurrent responses with M.SssI + Dpn I, Dam MTase alone and Dpn I alone were negligible.

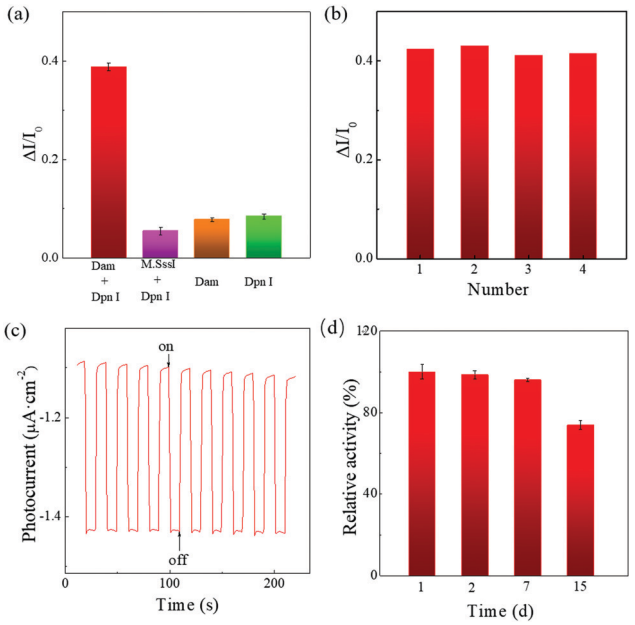

Fig. 7 (a) Photocurrent responses of the proposed PEC biosensor with Dam MTase + Dpn I, M.SssI MTase + Dpn I, Dam, or Dpn I under the same experimental conditions. (b) Reproducibility of the PEC biosensor in the presence of 100 U mL^{-1} Dam MTase. (c) Stability of the proposed biosensor incubated with 100 U mL^{-1} Dam MTase under several on/off irradiation cycles for 200 s. (d) Stability of the PEC biosensor for the Dam MTase (10 U mL^{-1}) assay after 1, 2, 7, and 15 days.

These results successfully verified that the constructed PEC biosensor has unique selectivity and specificity for the Dam MTase assay.

The reproducibility of the proposed PEC biosensor was studied by determining 100 U mL^{-1} Dam MTase using four independent sensors (Fig. 7b). The proposed PEC biosensors exhibited excellent reproducibility with a minor relative standard deviation (RSD) of 1.8%.

In addition, to demonstrate the stability of the constructed PEC biosensor, we detected the photocurrent under several continuous on/off irradiation cycles for 200 s after S1-Au NPs were captured. As shown in Fig. 7c, the PEC biosensor showed a stable photocurrent response, proving that the stability of the PEC biosensor was excellent. Moreover, to further confirm the reliability and stability of the biosensor, the prepared PEC biosensor (S1-Au NPs/Dpn I/Dam MTase/hDNA/Sb_2Se_3–GO/ITO) with 10 U mL^{-1} Dam MTase in 10 mM PBS (pH 7.4) was stored at 4 °C and retained 98%, 96%, and 74% of the initial response after storage for 2, 7, and 15 days (Fig. 7d), respectively, indicating that the constructed PEC biosensor had satisfactory reliability and stability.

Preliminary analysis of real samples

To evaluate the reliability of the constructed PEC biosensor, three different concentrations of Dam MTase (0.001, 1, or 100 U mL^{-1}) were spiked into healthy human serum. As listed in Table 2, the as-fabricated biosensors showed good recovery in the range from 97.12% to 109.7%, and the RSD was less than 8.33%, suggesting that the PEC biosensor had good sensitivity and reliability for the detection of Dam MTase in real serum samples and could be used for clinical sample detection.

Table 2 Recovery tests of Dam MTase in serum samples

Sample	Added (U mL^{-1})	Found (U mL^{-1})	RSD (%)	Recovery (%)
1	1.00×10^{-3}	1.097×10^{-3}	1.75	109.7
2	1.00	1.026	3.39	102.6
3	100	97.12	8.33	97.12

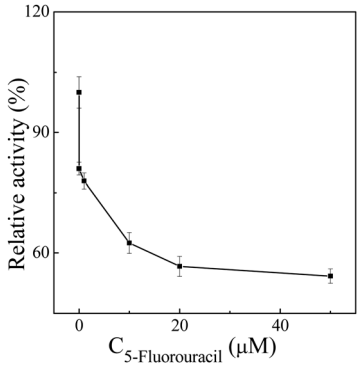

Fig. 8 Influence of inhibitor on Dam MTase activity.

Screening of Dam MTase inhibitors

The effect of the inhibitor concentration on the activity of Dam MTase was subsequently studied. 5-Fluorouracil, an anticancer drug, was selected as a model inhibitor to investigate the feasibility of our developed method for screening inhibitors; such a technique might be helpful for drug discovery. As shown in Fig. 8, the relative activity of Dam MTase decreased with increasing concentrations of 5-fluorouracil. Because the higher the concentration of 5-fluorouracil, the more Dam MTase activity can be inhibited, the shearing effect of Dpn I decreased with increasing 5-fluorouracil concentration, which reduced the capture of S1-Au NPs. Thus, the photoelectric signal decreased with increasing 5-fluorouracil concentration. This result showed that 5-fluorouracil had a significant dose-dependent inhibition of DNA methylation. Therefore, our established PEC biosensor was suitable for the inhibition analysis of Dam MTase activity.

Conclusion

In summary, we have fabricated a novel PEC biosensor by using Sb_2Se_3–GO as both the PEC probe and substrate for biomolecule conjugation, and Au NPs as a quencher based on the competitive absorption of light and strong EET between Sb_2Se_3 and Au NPs for the highly sensitive detection of Dam MTase. Compared with the traditional semiconductors such as CdTe, the photoelectrically active material Sb_2Se_3–GO possessed the following advantages. Firstly, Sb_2Se_3 was stable, non-toxic and low cost, a highly desirable factor for biosensing applications. Secondly, the coupling of Sb_2Se_3 with GO resulted in higher biocompatibility and more active sites for biomolecule conjugation, which was crucial for sensing signal amplification. As a result, the

constructed PEC sensor exhibited a broad linear detection range of 0.001–100 U mL^{-1} and a detection limit of 0.6 mU mL^{-1}, which was comparable and even superior to those in previous reports. The high sensitivity was ascribed to the unique photoelectric properties of Sb_2Se_3 and the efficient quenching of Au NPs towards Sb_2Se_3. This work provides an alternative to Sb_2Se_3 as a promising PEC probe for biosensing with merits including large-scale and convenient synthesis, high photoelectric activity and stability in potential applications.

Experimental

Reagents

Dam MTase, *S*-adenosyl methionine (SAM), Dpn I endonuclease, and M.SssI methyltransferase (M.SssI MTase) were purchased from New England Biolabs (Ipswich, MA, USA). Hairpin DNA (hDNA, 5′-CAGAGATCCATATACGTTTTTCGTATATGGATCTCTGAAAAA-$(CH_2)_6$-NH_2-3′), S1 (5′-TTTTTCAGAGA$(CH_2)_6$-SH-3′) and phosphate buffer solution (PBS) were obtained from Sangon Biotech (Shanghai, China). Selenium powder (Se), antimony(III) chloride ($SbCl_3$), thioglycolic acid (TGA), ethanolamine (EA), gold(III) chloride trihydrate ($HAuCl_4{\cdot}3H_2O$), 2-methoxyethanol (2-ME), 1-ethyl-3-(3-dimethylaminopropyl)carbodiimide hydrochloride (EDC), chitosan (CS), and *N*-hydroxysuccinimide (NHS) were received from Sigma-Aldrich (USA). Graphene oxide (GO) was prepared by a modified Hummers' method using graphite flakes as the precursor.[36] β-Mercaptoethanol (MCH) was supplied by Macklin Biochemical Technology Co., Ltd (Shanghai, China). Trisodium citrate ($Na_3C_6H_5O_7$), potassium ferricyanide ($K_3[Fe(CN)_6]$) and potassium ferrocyanide ($K_4[Fe(CN)_6]$) were obtained from Shanghai Lingfeng Chemical Reagent Co., Ltd (Shanghai, China). Indium tin oxide (ITO, 6.2–6.8 Ω sq^{-1}) slices were received from Zhuhai Kaivo Optoelectronic Technology Corporation (Zhuhai, China). Other chemicals, such as ascorbic acid (AA), acetone, ammonia, and ethanol, were purchased from Sinopharm Chemical Reagent Co., Ltd (Shanghai, China). All chemical reagents used in this experiment were of analytical grade unless otherwise specified. Ultrapure water (18.2 MΩ cm, Milli-Q) was used in all experiments.

Apparatus

The ultraviolet-visible (UV-vis) absorption spectra were recorded using a Cary100 UV-vis spectrophotometer (Agilent, Singapore). Scanning electron microscopy (SEM) images were collected using a Zeiss Ultra Plus (Germany). Transmission electron microscopy (TEM) was conducted using a H-600-4 transmission electron microscope (Hitachi, Japan). X-ray photoelectron spectroscopy (XPS) was performed on a Thermo ESCALAB 250XI system. Fluorescence spectra were recorded on a FluoroMax-4 spectrofluorometer with xenon discharge lamp excitation (Horiba, Japan). Cyclic voltammetry (CV) and PEC measurements were performed on a CHI 660e electrochemical workstation (CH Instruments, Shanghai, China) at room temperature. All electrochemical characterization was performed by using a three-electrode system: a modified ITO electrode with an area of 0.16 cm^2 was used as the working electrode, a Ag/AgCl (KCl-saturated) electrode was used as the reference electrode, and a platinum wire was used as the counter electrode. PBS buffer (0.01 M, pH = 6) containing 0.1 M AA was used as the PEC electrolyte.[37,38] A 150 W xenon lamp was utilized as the source of visible light (Zolix Instruments CO., Ltd, Beijing, China) for PEC measurements.

Synthesis of Sb_2Se_3 and Sb_2Se_3–GO complexes

Sb_2Se_3 nanostructures were synthesized according to a previous report[11] with some modification. Briefly, 0.405 g of Se powder, 0.46 mL of TGA, and 7.54 mL of EA were added to a mixture containing 0.1 M $SbCl_3$ and 12 mL of 2-ME with magnetic stirring at 80 °C overnight. The solution was deoxygenated with nitrogen for 10 min before the reaction. Finally, the product was washed successively with ethanol and ultrapure water and dried to obtain Sb_2Se_3. The Sb_2Se_3–GO nanohybrid was prepared by mixing different molar ratios of Sb_2Se_3 and GO and sonicating for 2 h.

Fabrication of Au NPs and further conjugation with S1

Gold nanoparticles (Au NPs) were prepared according to previous literature.[39] A total of 34 mL of 0.01% $HAuCl_4{\cdot}3H_2O$ solution was heated to boiling, and 38.8 mM $Na_3C_6H_5O_7$ solution was added. The mixture was reacted for 15 min and cooled to room temperature. The as-prepared Au NPs were conjugated with 10 μL of 100 μM S1, and the mixture was then stirred for 12 h at 4 °C.

PEC biosensor assay procedure

ITO electrodes were successively immersed in acetone, ethanol and water, ultrasonically cleaned for 20 min, and then blown dry with nitrogen. Subsequently, a mixture of 10 μL of as-obtained Sb_2Se_3–GO and CS (0.05 wt%) was dropped onto an ITO slice and dried in air for 18 h. Then, 10 μL of a mixed solution consisting of EDC (20 mg mL^{-1}) and NHS (10 mg mL^{-1}) was dropped onto the obtained Sb_2Se_3–GO/ITO for 1 h. An activated Sb_2Se_3–GO/ITO electrode was obtained after washing with PBS (0.01 M, pH = 7.4) to remove the excess EDC and NHS. After that, 10 μL of annealed hDNA (10 μg mL^{-1}) was incubated on the surface of the electrode at 4 °C for 12 h. Following rinsing with PBS, 10 μL of 2 mM MCH solution was added to the hDNA/Sb_2Se_3–GO/ITO electrode and incubated at 37 °C for 40 min to block the nonspecific binding sites. Then, 10 μL of different concentrations of Dam MTase containing appropriate buffer was added to the methylation reaction system and incubated at 37 °C for 2 h. Afterward, 10 μL of Dpn I (10 U mL^{-1}) containing appropriate buffer was added to the modified ITO electrode, and the mixture was incubated at 37 °C for 2 h. Finally, 10 μL of the as-prepared S1-Au NP solution was dropped onto the above modified ITO electrode and incubated at 37 °C for 2 h. The Dam MTase biosensor was thus obtained by rinsing with PBS (0.01 M, pH = 7.4).

Detection of Dam MTase in serum

Serum collected from healthy individuals was diluted 10-fold with 10 mM PBS (pH = 7.4). The serum samples were spiked with Dam MTase at 0.001, 1, and 100 U mL^{-1} for the recovery test. Then, these samples were analyzed by the constructed PEC

biosensor, and each spiked sample was analyzed with four sets of parallel controls. The final concentration of spiked samples was calculated according to the standard calibration curve.

Influence of an inhibitor on Dam MTase activity

The influence of different concentrations of inhibitor on Dam MTase activity was analyzed by using 5-fluorouracil as an inhibitor to demonstrate the potential application of the developed PEC assay. The inhibitor assay process was similar to the detection of Dam MTase. The inhibitor assay mixture contained 100 U mL^{-1} Dam MTase, 80 μM SAM, 1× Dam buffer and various concentrations of the inhibitor.

Conflicts of interest

There are no conflicts of interest to declare.

Acknowledgements

This work is supported by the National Natural Science Foundation of China (21675022 and 21775018), Program from the Natural Science Foundation of Jiangsu Province (BK20170084 and BK20160028) and the Fundamental Research Funds for the Central Universities (2242019K3DN04 and 2242019K41036).

Notes and references

1 A. Jeltsch, *ChemBioChem*, 2002, **3**, 274.
2 S. Y. Chen, Y. Q. Lv, Y. F. Shen and Y. J. Zhang, *ACS Appl. Mater. Interfaces*, 2018, **10**, 6887.
3 R. J. Acton and C. G. Bell, *AME Med. J.*, 2017, **2**, 110.
4 A. Bergerat, W. Guschlbauer and G. V. Fazakerley, *Proc. Natl. Acad. Sci. U. S. A.*, 1991, **88**, 6394.
5 L. Li, L. Tao, R. A. Lubet, V. E. Steele and M. A. Pereira, *Carcinogenesis*, 2007, **28**, 1499.
6 G. W. S. L. Rebeck, *J. Bacteriol.*, 1991, **173**, 2068.
7 S. Saha, Y. Chan and L. Soleymani, *ACS Appl. Mater. Interfaces*, 2018, **10**, 31178.
8 R. Zeng, Z. Luo, L. Su, L. Zhang, D. Tang, R. Niessner and D. Knopp, *Anal. Chem.*, 2019, **91**, 2447.
9 H. Y. Wang, L. B. Zhu, J. L. Duan, M. H. Wang, H. S. Yin, P. Wang and S. Y. Ai, *Biosens. Bioelectron.*, 2018, **103**, 32.
10 H. J. Xue, J. J. Zhao, Q. Zhou, D. Pan, Y. Zhang, Y. J. Zhang and Y. F. Shen, *ACS Appl. Nano Mater.*, 2019, **2**, 1579.
11 W. Yang, S. Lee, H. Kwon, J. Tan, H. Lee, J. Park, Y. Oh, H. Choi and J. Moon, *ACS Nano*, 2018, **12**, 11088.
12 W. Yang, J. Ahn, Y. Oh, J. Tan, H. Lee, J. Park, H. Kwon, J. Kim, W. Jo, J. Kim and J. Moon, *Adv. Energy Mater.*, 2018, **8**, 1702888.
13 M. L. Huang, P. Xu, D. Han, J. Tang and S. Y. Chen, *ACS Appl. Mater. Interfaces*, 2019, **11**, 15564.
14 C. Chen, Y. Zhao, S. C. Lu, K. H. Li, Y. Li, B. Yang, W. H. Chen, L. Wang, D. B. Li, H. Deng, F. Yi and J. Tang, *Adv. Energy Mater.*, 2017, **7**, 1700866.
15 Y. Zhou, L. Wang, S. Chen, S. Qin, X. S. Liu, J. Chen, D. J. Xue, M. Luo, Y. Z. Cao, Y. B. Cheng, E. H. Sargent and J. Tang, *Nat. Photonics*, 2015, **9**, 409.
16 L. Wang, D. B. Li, K. H. Li, C. Chen, H. X. Deng, L. Gao, Y. Zhao, F. Jiang, L. Y. Li, F. Huang, Y. He, H. S. Song, G. D. Niu and J. Tang, *Nat. Energy*, 2017, **2**, 1.
17 J. Kim, W. Yang, Y. Oh, H. Lee, S. Lee, H. Shin, J. Kim and J. Moon, *J. Mater. Chem. A*, 2017, **5**, 2180.
18 X. S. Liu, J. Chen, M. Luo, M. Y. Leng, Z. Xia, Y. Zhou, S. Qin, D. J. Xue, L. Lv, H. Huang, D. M. Niu and J. Tang, *ACS Appl. Mater. Interfaces*, 2014, **6**, 10687.
19 A. Z. Liao, Y. Zhou, L. X. Xiao, C. F. Zhang, C. P. Wu, A. M. Asiri, M. Xiao and Z. G. Zou, *Nanoscale*, 2018, **11**, 109.
20 L. Yu, J. Chen and Z. W. Fu, *Electrochim. Acta*, 2010, **55**, 1258.
21 Q. Zhou, H. J. Xue, Y. Y. Zhang, Y. Q. Lv, H. G. Li, S. Q. Liu, Y. F. Shen and Y. J. Zhang, *ACS Sens.*, 2018, **3**, 1385.
22 X. Ou, C. H. Yang, X. H. Xiong, F. H. Zheng, Q. C. Pan, C. Jin, M. L. Liu and K. Huang, *Adv. Funct. Mater.*, 2017, **27**, 1606242.
23 Y. Lu and J. W. Liu, *Nat. Protoc.*, 2006, **1**, 246.
24 Q. M. Shen, L. Han, G. C. Fan, E. S. Abdel-Halim, L. P. Jiang and J. J. Zhu, *Biosens. Bioelectron.*, 2015, **64**, 449.
25 X. R. Zhang, Y. Zhang, F. T. Chen, Y. Lia and S. S. Zhang, *Chem. Commun.*, 2016, **52**, 13261.
26 X. F. Wei, X. M. Ma, J. J. Sun, Z. Y. Lin, L. H. Guo, B. Qiu and G. N. Chen, *Anal. Chem.*, 2014, **86**, 3563.
27 Y. Chen, X. Z. Meng, H. W. Gu, H. C. Yi and W. Y. Sun, *Biosens. Bioelectron.*, 2019, **134**, 117.
28 Y. X. Zhao, F. Chen, Y. Y. Wu, Y. H. Dong and C. H. Fan, *Biosens. Bioelectron.*, 2013, **42**, 56.
29 X. W. Xu, L. Wang, X. Li, W. L. Cui and W. Jiang, *Talanta*, 2019, **194**, 282.
30 S. Bi, T. T. Zhao, B. Y. Luo and J. J. Zhu, *Chem. Commun.*, 2013, **49**, 6906.
31 Y. H. Wang, X. X. He, K. M. Wang, J. Su, Z. F. Chen, G. P. Yan and Y. D. Du, *Biosens. Bioelectron.*, 2013, **41**, 238.
32 X. E. Luo, Y. Li, J. B. Zheng, H. Qi, Z. X. Liang and X. H. Ning, *Chem. Commun.*, 2015, **51**, 9487.
33 J. J. Ge, Y. Zhao, C. L. Li and G. F. Jie, *Anal. Chem.*, 2019, **91**, 3546.
34 X. L. Peng, J. L. Zhu, W. Wen, T. Bao, X. H. Zhang, H. P. He and S. F. Wang, *Biosens. Bioelectron.*, 2018, **118**, 174.
35 H. Y. Li, J. Wang, X. Wang, H. Y. Lin and F. Li, *ACS Appl. Mater. Interfaces*, 2019, **11**, 16958.
36 Y. J. Zhang, K. Fugane, T. Mori, L. Niu and J. H. Ye, *J. Mater. Chem.*, 2012, **22**, 6575.
37 G. Wang, P. Yu, J. Xu and H. Chen, *J. Phys. Chem. C*, 2009, **113**, 11142.
38 L. Mi, P. Y. Wang, J. R. Yan, J. Qian, J. H. Lu, J. C. Yu, Y. H. Wang, H. Liu, M. Zhu, Y. K. Wan and S. Q. Liu, *Anal. Chim. Acta*, 2016, **902**, 107.
39 M. M. Zhang, G. H. Li, Q. Zhou, D. Pan, M. Zhu, R. Y. Xiao, Y. J. Zhang, G. Q. Wu, Y. K. Wan and Y. F. Shen, *ACS Sensors*, 2018, **3**, 684.